Journal of Mathematics Research; Vol. 14, No. 1; February 2022
ISSN 1916-9795 E-ISSN 1916-9809
Published by Canadian Center of Science and Education

An Advanced Galerkin Approach to Solve the Nonlinear Reaction-Diffusion Equations With Different Boundary Conditions

Hazrat Ali[1], Md. Kamrujjaman [2], & Md. Shafiqul Islam[1]

[1] Department of Applied Mathematics, University of Dhaka, Dhaka 1000, Bangladesh

[2] Department of Mathematics, University of Dhaka, Dhaka 1000, Bangladesh

Correspondence: Md. Kamrujjaman, Department of Mathematics, University of Dhaka, Dhaka 1000, Bangladesh

Received: November 30, 2021 Accepted: December 31, 2021 Online Published: January 14, 2022

doi:10.5539/jmr.v14n1p30 URL: https://doi.org/10.5539/jmr.v14n1p30

Abstract

This study proposed a scheme originated from the Galerkin finite element method (GFEM) for solving nonlinear parabolic partial differential equations (PDEs) numerically with initial and different types of boundary conditions. The scheme is applied generally handling the nonlinear terms in a simple way and throwing over restrictive assumptions. The convergence and stability analysis of the method are derived. The error of the method is estimated. In the series, eminent problems are solved, such as Fisher's equation, Newell-Whitehead-Segel equation, Burger's equation, and Burgers-Huxley equation to demonstrate the validity, efficiency, accuracy, simplicity and applicability of this scheme. In each example, the comparison results are presented both numerically and graphically.

Keywords: Burger's equation, Burgers-Huxley equation, Convergence analysis, GFEM, Newell-Whitehead-Segel equation

1. Introduction

In this paper, we consider a standard form of nonlinear parabolic partial differential equations (PDEs) in the following way defined on the spatio-temporal domain, $\mathcal{R} = \Lambda \times (0, T],\ T > 0$

$$\frac{\partial A(x,t)}{\partial t} = \eta \frac{\partial^2 A(x,t)}{\partial x^2} + \Psi\left(x, t, A(x,t), \frac{\partial A(x,t)}{\partial x}\right), \quad (x,t) \in \mathcal{R}. \tag{1}$$

The initial condition is defined as

$$A(x,0) = \Theta(x), \qquad x \in \Lambda, \tag{2}$$

subject to the boundary conditions

$$\begin{cases} \alpha_1 A(\ell_1, t) + \beta_1 \dfrac{\partial A(\ell_1,t)}{\partial x} = \gamma_1, & (x,t) \in \partial\mathcal{R}, \\ \alpha_2 A(\ell_2, t) + \beta_2 \dfrac{\partial A(\ell_2,t)}{\partial x} = \gamma_2, & (x,t) \in \partial\mathcal{R}, \end{cases} \tag{3}$$

where $\eta > 0$ is the diffusion coefficient, x is the space, and t, the time. The variable A is the function of time, t and space, x. The initial condition $A(x,0) = \Theta$ describes the function of the spatial variable, x. The notation Λ is a region bounded in $\mathbb{R}^j$, typically $j = \{1,2,3\}$, with boundary $\partial\Lambda \in C^{2+\delta},\ 0 < \delta < 1$. The function Ψ presents the reaction-advection map (either reaction or advection or both of them simultaneously). The reaction function is smooth enough, i.e. Ψ is continuous and at least first partial derivative exist. The advection term is defined as $\frac{\partial A}{\partial x}$ in (1). The notations $\alpha_i \in \mathbb{R},\ \beta_i \in \mathbb{R},\ \gamma_i \in \mathbb{R}\ (i = 1,2)$ are constants and either $\alpha_1 = \alpha_2 = 0$ or, $\beta_1 = \beta_2 = 0$. It is noted that α_1 and β_1 both are not zero at the same time. Similarly α_2 and β_2 are not zero simultaneously. The left and right boundary points are ℓ_1 and ℓ_2 respectively and both $\ell_1,\ \ell_2 \in \mathbb{R}$. Also, in this study Ψ and Θ describe the nonlinear function of $A(x,t)$ and x, respectively. It is also remarked that in many cases, $\Theta(x)$ can be linear steady state. The boundary conditions (3) cover a wide class depending on the parameters, for example:

1. Dirichlet boundary conditions if $\beta_1 \equiv \beta_2 \equiv 0$, and $\alpha_1 \not\equiv \alpha_2 \not\equiv 0$,
2. Neumann boundary conditions if $\alpha_1 \equiv \alpha_2 \equiv 0$, and $\beta_1 \not\equiv \beta_2 \not\equiv 0$,

3. Robin boundary conditions for all non-zero parameters, $\alpha_1,\ \alpha_2,\ \beta_1$ and β_2.

The mixed boundary conditions are the next possibility based on proper parameters selection.

These types of nonlinear parabolic partial differential equations (PDEs) (1) frequently arise in the field of engineering and science. They are generally used to describe a wide variety of time-dependent phenomena. Some instantaneous applications are drawn in the following series (Mittal & Jain, 2012):

- particle diffusion and the modeling of turbulence,
- pricing of derivative investment instruments,
- filtration of liquids, gas dynamics and elasticity,
- modeling of biological species (organisms) with harvesting and Allee effect, and
- chemical reactions, environmental pollution etc.

So the solutions of those types of equations have great significance in science and engineering, see, (Ozis, Aksan & Ozdes, 2003; Caldwell, Wanless & Cook, 1981; Reddy, 2014; Rao, 2017; Lewis & Ward, 1991; Chen, 2005; Akter et al., 2020) and references therein. The analytic solutions of second or higher order nonlinear PDEs are not easy and impossible in many cases except some simple cases. Many difficulties encountered, such as the nature of the governing equation, to construct an appropriate mesh, complex geometrical shapes, ill conditions, and singularity problems. So researchers devoted their attention to developing new and efficient solution methodologies to solve those problems numerically.

Instead of analytic solutions, the scientists introduced robust numerical techniques to find an approximation of the solutions, and in this study, we were interested in numerical solutions. Numerous authors had proposed different types of numerical methods for solving nonlinear parabolic PDEs (Hassan & Rashidi, 2014; Sarwar & Rashidi, 2016). Jacques solved this type of equations by predictor-corrector method (Jacques, 1983). Mittal and Jain solved nonlinear parabolic PDEs by Cubic B-splines collocation method (Mittal & Jain, 2012) which is limited only for Neumann boundary conditions. As a consequence, Caldwell *et al.* applied a finite element approach to solve Burger's but linear equation (Caldwell, Wanless & Cook, 1981). After transforming the nonlinear parabolic PDE into linear PDE by Hopf-Cole transformation, Ozis *et al.* found the solutions of the Burger's equation by finite element method with homogeneous Neumann boundary conditions (Ozis, Aksan & Ozdes, 2003). During the solution process, they used the kinematics viscosity within $[0.004 - 0.01]$. Using the classical Lie approach with additional generating conditions method, Cherniha and Dutka established the analytic solution of the Fisher's equation (Cherniha & Dutka, 2001). Ali *et al.* used quadratic element method for solving fractional-order differential equation (Ali, Kamrujjaman & Shirin, 2021). At the initial time, they compared the exact and the numerical solutions found by the finite element method with local perturbations of the analytic solution. In this method, they replaced the infinite interval into a finite interval so that the method should satisfy the homogeneous Neumann boundary conditions with sufficient exactness in this minimal interval. Ali *et al.* used Galerkin finite element method for solving nonlinear ordinary differential equations (Ali & Islam, 2017) . The FitzHugh-Nagumo equation and several other nonlinear reaction-diffusion were solved using the standard linear shape functions for various parameter values (Ali, Kamrujjaman & Islam, 2020; Lima et al., 2020 & 2021; Ali & Kamrujjaman, 2021).

In this study, we have solved the nonlinear parabolic PDEs with various types of boundary conditions by our proposed scheme. In this method, different types of shape functions (linear, quadratic, cubic etc.) can be used instead of trial functions which are challenging to find that satisfy the boundary conditions; linear shape function is used in this paper with multiple nodes. In the literature, the current approach is not available as far as we know. So the main motive in this paper is to find the numerical solution of the nonlinear parabolic PDEs with different types of boundary conditions by our proposed scheme.

This paper comprises five sections. In Section , a proper derivation of our proposed scheme for nonlinear parabolic PDEs is formulated. The convergence and stability analysis along with the iterative procedures are discussed in Section . The implication of the method is presented in Section considering four problems with strong nonlinearity. Error graphs and numerical results are also presented in this Section. General discussion and concluding remarks can be found in Section .

In the following section, we are moving to discuss the key idea of our scheme that is based on Galerkin finite element method to solve nonlinear parabolic PDEs (1).

2. Mathematical Formulation

First of all, we span the domain $\mathcal{R}$ into n sub-domains. Let $\mathcal{S}_l$ be the $l-$th sub-domain of Λ with length $h\ (= \Delta x)$, which is the maximum length of all sub-domains and $k\ (= \Delta t)$ is the step length of t. An illustrative case as such is in Figure 1.

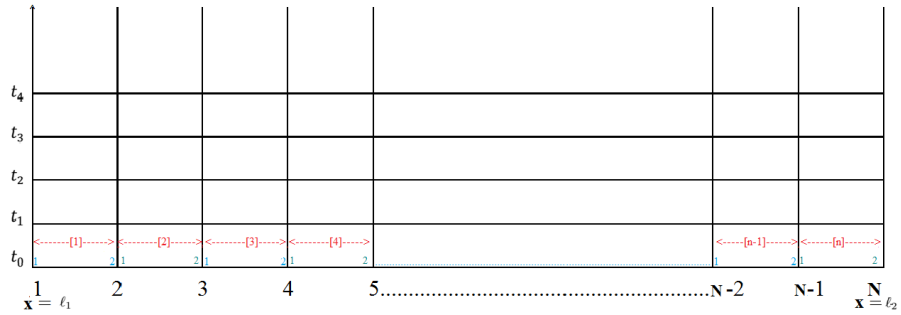

Figure 1. Domain discrimination for linear shape function at different times

If N is the total node number over the whole domain, then the total number of degrees of freedom over the domain is, $N = (\lambda - 1) \times n + 1$, where n is the total number of elements and λ is the local node number per element. The elements are numbered similarly with parenthesis $[e]$ (Ali & Islam, 2017) .

To find the solution, let us assume the trial solution

$$\tilde{a}(x,t) = \sum_{j=1}^{\lambda} a_j(t)\psi_j(x) \tag{4}$$

From the governing equation (1), the weighted residual equation for a particular element $[e]$ is

$$\int_{[e]} \left[\frac{\partial \tilde{a}}{\partial t} - \eta \frac{\partial^2 \tilde{a}}{\partial x^2} - \Psi\left(x, t, \tilde{a}, \frac{\partial \tilde{a}}{\partial x}\right) \right] \psi_i \, dx = 0,$$

which yields

$$\int_{[e]} \frac{\partial \tilde{a}}{\partial t}\psi_i \, dx + \eta \int_{[e]} \frac{\partial \psi_i}{\partial x}\frac{\partial \tilde{a}}{\partial x} \, dx - \int_{[e]} \Psi\left(x, t, \tilde{a}, \frac{\partial \tilde{a}}{\partial x}\right)\psi_i \, dx = \eta \left[\psi_i \frac{\partial \tilde{a}}{\partial x}\right]_{[e]}. \tag{5}$$

Where ψ_i $(i = 1, 2, 3, \cdots, \lambda)$ are the shape functions. After substituting $\tilde{a}(x,t)$, $\frac{\partial \tilde{a}(x,t)}{\partial x}$ from equation (4), we obtain

$$\int_{[e]} \left(\sum_{j=1}^{\lambda} \frac{\partial a_j(t)}{\partial t}\psi_j(x) \right)\psi_i(x)dx + \eta \int_{[e]} \frac{\partial \psi_i}{\partial x}\left(\sum_{j=1}^{\lambda} a_j(t)\frac{\partial \psi_j(x)}{\partial x} \right)dx$$

$$- \int_{[e]} \Psi\left[x, t, \left(\sum_{j=1}^{\lambda} a_j(t)\psi_j(x) \right), \left(\sum_{k=1}^{\lambda} a_j(t)\frac{\partial \psi_j(x)}{\partial x} \right) \right]\psi_i dx = \eta \left[\psi_i \sum_{j=1}^{\lambda} a_j(t)\frac{\partial \psi_j(x)}{\partial x} \right]_{[e]}$$

$$\Rightarrow \sum_{j=1}^{\lambda} \frac{\partial a_j(t)}{\partial t}\left(\int_{[e]} \psi_i(x)\psi_j(x)dx \right) + \sum_{j=1}^{\lambda} a_j(t)\left(\eta \int_{[e]} \frac{\partial \psi_i}{\partial x}\frac{\partial \psi_j(x)}{\partial x}dx \right)$$

$$- \sum_{j=1}^{\lambda} a_j(t)\left(\int_{[e]} \Psi\left(x, t, \sum_{k=1}^{\lambda} a_j(t)\frac{\partial \psi_j(x)}{\partial x} \right)\psi_i(x)\psi_j(x)dx \right) = \eta \left[\psi_i \left(\sum_{j=1}^{\lambda} a_j(t)\frac{\partial \psi_j(x)}{\partial x} \right) \right]_{[e]}$$

$$\Rightarrow \sum_{j=1}^{\lambda} \frac{\partial a_j(t)}{\partial t}\left(\int_{[e]} \psi_i(x)\psi_j(x)dx \right) + \sum_{j=1}^{\lambda} a_j(t) \int_{[e]} \left[\eta \frac{\partial \psi_i}{\partial x}\frac{\partial \psi_j(x)}{\partial x} - \Psi\left(x, t, \sum_{k=1}^{\lambda} a_j(t)\frac{\partial \psi_j(x)}{\partial x} \right)\psi_i(x)\psi_j(x) \right] dx$$

$$= \left[\eta\psi_i \left(\sum_{j=1}^{\lambda} a_j(t)\frac{\partial \psi_j(x)}{\partial x} \right) \right]_{[e]}$$

$$\Rightarrow \sum_{j=1}^{\lambda} \frac{\partial a_j(t)}{\partial t}\mathbf{C}_{ij}^e + \sum_{j=1}^{\lambda} a_j(t)\mathbf{K}_{ij}^e = F_i^e \tag{6}$$

The last equation is the matrix form of the system of ordinary differential equations with respect to t, where

$$\mathbf{C}_{ij}^{e} = \int_{[e]} \psi_i \psi_j \, dx \tag{7}$$

$$\mathbf{K}_{ij}^{e} = \int_{[e]} \left[\eta \frac{d\psi_i}{dx} \frac{d\psi_j}{dx} - \Psi\left(x, t, \psi_i, \sum_{k=1}^{n} \left(a_k(t) \frac{d\psi_k}{dx} \right) \right) \psi_i \right] dx \tag{8}$$

$$F_i^e = \left[\eta \psi_i \sum_{k=1}^{n} \left(a_k(t) \frac{d\psi_k}{dx} \right) \right]_{[e]}. \tag{9}$$

Equation (6) can be rewritten in a convenient matrix form as

$$\mathbf{C}^{[e]} \frac{da(t)}{dt} + \mathbf{K}^{[e]} a(t) = F^{[e]}. \tag{10}$$

Here $\mathbf{K}$ and $\mathbf{C}$ are called the *stiffness* and *forced matrices* and F is called the *load vector*. Since $\mathbf{C}$ is symmetric, it is also referred to as *damping matrix*.

To transform the ordinary differential equation (10) into a recurrent equation, lots of different methods are available in the literature. For good accuracy, it is imperative to choose an effective but generalized iterative method. So we choose the α-family of approximation instead of traditional finite difference method that comprises *forward difference*, *backward difference*, or *central difference* approaches.

In α-family of approximations, for different values of α, we find the following well-known numerical integration schemes (Reddy, 2014):

$$\alpha = \begin{cases} 0, & \text{the forward difference scheme; order of accuracy} = O(k) \\ \frac{1}{2}, & \text{the Crank-Nicolson scheme; order of accuracy} = O(k^2) \\ \frac{2}{3}, & \text{the Galerkin method; order of accuracy} = O(k^2) \\ 1, & \text{the backward difference scheme; order of accuracy} = O(k) \end{cases}$$

By applying α-family of approximation, we form a system of algebraic equations to take a sequence of time steps of length h from time level j to $j+1$.

Then equation (10) becomes

$$\left(\frac{\mathbf{C}^{[e]}}{k} + \alpha \mathbf{K}^{[e]} \right) a_{j+1} = \left(\frac{\mathbf{C}^{[e]}}{k} - (1-\alpha) \mathbf{K}^{[e]} \right) a_j + F_j^{[e]}. \tag{11}$$

After assembling over all elements, equation (11) will be

$$\begin{bmatrix} \bar{h}_{11}^1 & \bar{h}_{12}^1 & 0 & 0 & 0 & 0 & \dots & 0 \\ \bar{h}_{21}^1 & \bar{h}_{22}^1 + \bar{h}_{11}^2 & \bar{h}_{12}^2 & 0 & \vdots & \vdots & \vdots & 0 \\ 0 & \bar{h}_{21}^2 & \bar{h}_{22}^2 + \bar{h}_{11}^3 & \bar{h}_{12}^3 & 0 & \vdots & \vdots & \vdots \\ \vdots & 0 & 0 & \ddots & \ddots & \vdots & \vdots & \vdots \\ \vdots & \vdots & \vdots & \ddots & \ddots & \ddots & 0 & \vdots \\ \vdots & \vdots & \vdots & \vdots & \ddots & \bar{h}_{22}^{n-2} + \bar{h}_{11}^{n-1} & \bar{h}_{12}^{n-1} & 0 \\ \vdots & \vdots & \vdots & \vdots & 0 & \bar{h}_{21}^{n-1} & \bar{h}_{22}^{n-1} + \bar{h}_{11}^{n} & \bar{h}_{12}^{n} \\ 0 & \dots & 0 & 0 & 0 & 0 & \bar{h}_{21}^{n} & \bar{h}_{22}^{n} \end{bmatrix} \begin{bmatrix} a_1 \\ a_2 \\ a_3 \\ \vdots \\ \vdots \\ \vdots \\ a_n \\ a_{n+1} \end{bmatrix}_{j+1}$$

=

$$\begin{bmatrix} \hat{\mathrm{h}}_{11}^{1} & \hat{\mathrm{h}}_{12}^{1} & 0 & 0 & 0 & 0 & ... & 0 \\ \hat{\mathrm{h}}_{21}^{1} & \hat{\mathrm{h}}_{22}^{1}+\hat{\mathrm{h}}_{11}^{2} & \hat{\mathrm{h}}_{12}^{2} & 0 & \vdots & \vdots & \vdots & 0 \\ 0 & \hat{\mathrm{h}}_{21}^{2} & \hat{\mathrm{h}}_{22}^{2}+\hat{\mathrm{h}}_{11}^{3} & \hat{\mathrm{h}}_{12}^{3} & 0 & \vdots & \vdots & \vdots \\ \vdots & 0 & 0 & \ddots & \ddots & \vdots & \vdots & \vdots \\ \vdots & \vdots & \vdots & \ddots & \ddots & \ddots & 0 & \vdots \\ \vdots & \vdots & \vdots & \vdots & \ddots & \hat{\mathrm{h}}_{22}^{n-2}+\hat{\mathrm{h}}_{11}^{n-1} & \hat{\mathrm{h}}_{12}^{n-1} & 0 \\ \vdots & \vdots & \vdots & \vdots & 0 & \hat{\mathrm{h}}_{21}^{n-1} & \hat{\mathrm{h}}_{22}^{n-1}+\hat{\mathrm{h}}_{11}^{n} & \hat{\mathrm{h}}_{12}^{n} \\ 0 & ... & 0 & 0 & 0 & 0 & \hat{\mathrm{h}}_{21}^{n} & \hat{\mathrm{h}}_{22}^{n} \end{bmatrix} \begin{bmatrix} a_1 \\ a_2 \\ a_3 \\ \vdots \\ \vdots \\ \vdots \\ a_n \\ a_{n+1} \end{bmatrix}_j + \begin{bmatrix} \bar{f}_1^1 \\ \bar{f}_2^1+\bar{f}_1^2 \\ \bar{f}_2^2+\bar{f}_1^3 \\ \vdots \\ \vdots \\ \vdots \\ \bar{f}_2^{n-1}+\bar{f}_1^n \\ \bar{f}_2^n \end{bmatrix}_j .$$

Which can be written as

$$\left[\bar{\mathbb{H}}\right]\{a\}_{j+1} = [\hat{\mathbb{H}}]\{a\}_j + \left\{\bar{\mathbb{F}}\right\}_j . \tag{12}$$

Where the triangular matrices $\left[\bar{\mathbb{H}}\right]$ & $[\hat{\mathbb{H}}]$ are $N \times N$ and the vectors $\left\{\bar{\mathbb{F}}\right\}_j$ is an $N \times 1$ in sizes, whose entries are as follows:

$$\bar{\mathrm{h}}_{ij}^{[e]} = \frac{\mathbf{C}_{ij}^{[e]}}{h} + \alpha \mathbf{K}_{ij}^{[e]} \tag{13}$$

$$\hat{\mathrm{h}}_{ij}^{[e]} = \frac{\mathbf{C}_{ij}^{[e]}}{h} - (1-\alpha)\mathbf{K}_{ij}^{[e]} \tag{14}$$

$$\bar{f}_i^{[e]} = F_i^{[e]}. \tag{15}$$

However, to treat the nonlinearity, we convert the nonlinear term as a multiple of $A(x,t)$ to express in matrix form. Which we transform as a function of a_j by using equation (4). Applying the initial condition into the recurrent equation (12), we iterate to find a better approximation for a particular time t. Putting back the values of a_j for a particular element in equation (4), we find a piece-wise function of space and time for that element. Using the previously obtained function, we can find values of $A(x,t)$ at any point on the element for a particular time t. Next Section contains one important branch of this study, the convergence and stability analysis which ensures that our method is convergent and our iterative procedure is stable for small time steps.

3. Convergence and Stability Analysis

Let the shape functions are $\psi_j(x) \in H_2^1, j = 1, 2, \cdots, \lambda$ where H_2^1 is the Hilbert space. Since η is a constant and $\Psi\left(x, t, A(x,t), \frac{\partial A(x,t)}{\partial x}\right)$ is continuous functions, so the solution of equation (1) uniquely exist (Babuska & Rheinboldt, 1978). Now substitute the trial function from equation (4) into (1), then we find equation (10) as

$$\left\{\frac{da(t)}{dt}\right\} + [\mathbf{C}]^{-1}[\mathbf{K}]\{a(t)\} = [\mathbf{C}]^{-1}\{F\}. \tag{16}$$

Equation (16) is an initial value problem

$$\begin{aligned} &\frac{da_j}{dt} + \zeta_j a_j = \Im_j, \\ &a_j(0) = \phi(x). \end{aligned} \tag{17}$$

The integrating factor of equation (17) is

$$e^{\int \zeta_j dt} = e^{\zeta_j t}.$$

Multiplying on both sides of the first equation of (17) by integrating factor and then integrating over $(0, T]$, we have

$$\begin{aligned} e^{\zeta_j t} a_j &= \int_0^T e^{\zeta_j \mathfrak{x}} \Im_j(\mathfrak{x}) d\mathfrak{x} \\ \Rightarrow a_j &= e^{-\zeta_j t} \int_0^T e^{\zeta_j \mathfrak{x}} \Im_j(\mathfrak{x}) d\mathfrak{x} = \int_0^T e^{-\zeta_j (t-\mathfrak{x})} \Im_j(\mathfrak{x}) d\mathfrak{x}, \end{aligned} \tag{18}$$

and

$$|a_j|^2 \leq \frac{1}{2\zeta_j} \int_0^T |\Im_j(\mathfrak{x})|^2 d\mathfrak{x}. \tag{19}$$

So in energy norm for a fixed t, we have

$$\left\|\tilde{A}(x,t)\right\|_E^2 = \sum_{j=1}^{\lambda} |a_j(t)|^2 \zeta_j$$

$$\Rightarrow \left\|\tilde{A}(x,t)\right\|_E^2 \leq \sum_{j=1}^{\lambda} \left(\frac{1}{2\zeta_j} \int_0^T |\Im_j(\mathfrak{x})|^2 d\mathfrak{x}\right) \zeta_j = \sum_{j=1}^{\lambda} \left(\frac{1}{2} \int_0^T |\Im_j(\mathfrak{x})|^2 d\mathfrak{x}\right).$$

Therefore, the series in equation (4) converges for a specific value of t.

Let $\mathscr{D}^{p,q}$ be the space of $(p-1)$ times continuously differentiable functions on $\bar{\Lambda}$, the closure of the domain, for which the restriction to Λ_j, $j = 0, 1, 2, \cdots, n-1$ is a polynomial of degree at most $\lambda - 1$, where λ is the number of local nodes in each element. Let $\tilde{A} \in \mathscr{D}^{p,q}$ be the finite element solution for a particular value of t, then for all $\upsilon \in \mathscr{D}^{p,q}$

$$\left(\frac{\partial \tilde{A}}{\partial t}, \upsilon\right)_0 + \mathcal{B}\left(\tilde{A}, \upsilon\right) = (F, \upsilon)_0, \tag{20}$$

where $(.,.)_0$ is the inner product and $\mathcal{B}(.,.)$ is the bilinear transformation defined in (Babuska & Rheinboldt, 1978; Babuska, 1972). Equation (20) provides an initial value problem instead of the system of ordinary differential equations. It is well known that for decreasing the increments in x, this result will converge to the solution of equation (10) for a particular t.

Now the iterative schemes can be applied in a relaxed way, if it is numerically stable. So write equation (12) as

$$\left[\bar{\mathbb{H}}\right]\{a\}_{j+1} = [\hat{\mathbb{H}}]\{a\}_j + \left\{\bar{\mathbb{F}}\right\}_j \tag{21}$$

$$\{a\}_{j+1} = [\mathbb{A}]\{a\}_j + \left[\bar{\mathbb{H}}\right]^{-1}\left\{\bar{\mathbb{F}}\right\}_j, \tag{22}$$

where $[\mathbb{A}] = \left[\bar{\mathbb{H}}\right]^{-1}[\hat{\mathbb{H}}]$ is the amplification matrix. Here $\{a\}_{j+1}$, $\{a\}_j$ are the solution vector at time $(t+1)$ and t, respectively.

The solution $\{a\}_{j+1}$ at time $(t+1)$ relies on the solution $\{a\}_j$ at time t. So error can grow with iteration. An iterative method is said to be stable if the error does not grow in an unbounded way with iteration. The necessary and sufficient conditions to bound the error within a borderline, the eigenvalue χ_{max} of the amplification matrix $[\mathbb{A}]$ must be less or equal unity such that

$$([\mathbb{A}] - \chi_{max}[I])\{a\} = 0. \tag{23}$$

Equation (23) is an eigenvalue problem which is *unconditionally stable* if χ_{max} is less or equal to unity for any time steps k (Reddy,2014). If χ_{max} depends on the step size of time to be less or equal unity, then the procedure will be called *conditionally stable*. Thus α-family of approximation for $\alpha < \frac{1}{2}$, all numerical schemes are stable for the time increment which satisfies the condition that is written as

$$k < \frac{2}{(1-2\alpha)\chi_{max}}. \tag{24}$$

And for $\alpha \geq \frac{1}{2}$, the largest eigenvalue of the amplification matrix satisfies the following inequality

$$\chi_{max} = \|\frac{1-(1-\alpha)k\chi_{max}}{1+\alpha k\chi_{max}}\| \leq 1, \tag{25}$$

which reveals that α-family of approximation is unconditionally stable if $\alpha \geq \frac{1}{2}$.

In the following Section , we are going to present the solution of several nonlinear parabolic PDEs to demonstrate the efficiency of this method. Also, we will study the role played among different parametric values, exact-approximate solution, number of linear elements, and error terms while time varies.

4. Numerical Examples and Applications

In this section, the solutions of some re-known nonlinear parabolic equations with different boundary conditions are considered. All results are presented graphically and numerically, along with the exact solution.

4.1 Burger's Equation

Nonlinear Burger's equation is one of the most famous equations that frequently raised in fluid dynamics, magnetohydrodynamics, etc. Here we solve this by our proposed scheme with homogeneous Dirichlet boundary conditions (Wood, 2006) and the problem is

$$\begin{cases} \dfrac{\partial A(x,t)}{\partial t} = \dfrac{1}{Re}\dfrac{\partial^2 A(x,t)}{\partial x^2} - A(x,t)\dfrac{\partial A(x,t)}{\partial x}, & x \in \Lambda \equiv [0,1], \quad t > 0, \\ A(0,t) = A(1,t) = 0, & t > 0, \quad x \in \partial\Lambda, \\ A(x,0) = \dfrac{2\pi \sin(\pi x)}{Re\,(\sigma + \cos(\pi x))}, & x \in \Lambda, \end{cases} \tag{26}$$

where $Re > 0$ is the Reynolds number and $\sigma > 1$ is a parameter. The analytic solution of the problem (26) is

$$A(x,t) = \frac{2e^{\frac{-\pi^2 t}{Re}} \sin(\pi x)}{Re\left(\sigma + e^{\frac{-\pi^2 t}{Re}} \cos(\pi x)\right)}.$$

For computation, we use only 40 linear elements with $Re = 1$, $\sigma = 2$, $k = 0.01$, $h = 0.025$, and $\alpha = 0.5$. The numerical results are presented numerically in Table 3 (Appendix A). The graphical parallelism between the exact and approximate solutions are depicted in Figure 2 and in Figure 4.

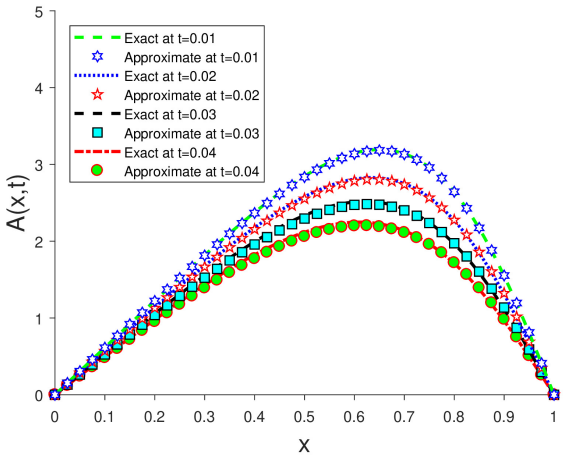

Figure 2. Comparison of the exact and approximate solutions of (26) over the domain while time varies

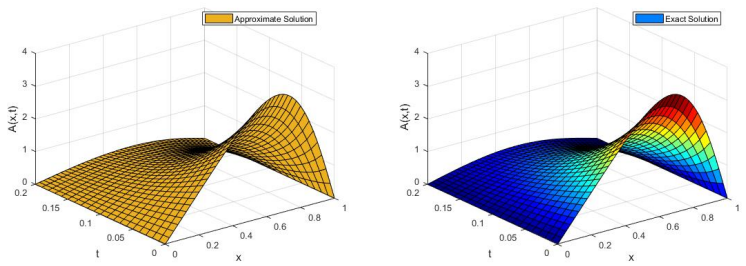

Figure 3. Approximate and exact solutions of (26) over the domain while time varies

To clarify the understanding, let us consider the three dimensional surface plot, Figure 3 of the Burger's equation (26). Compared with left and right diagrams in Figure 3, it is clear that the method is more suitable to solve such nonlinear parabolic PDEs without any complexity.

Figure 4 exhibits the corresponding difference between two graphs of approximate and exact solutions where the error term is very negligible. They also ensure the accuracy of the solution and acceptance of the proposed scheme.

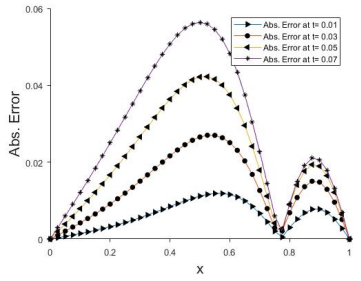

Figure 4. Absolute error of (26) over the domain while time varies

4.2 Fisher's Equation

In this illustration, we consider the renowned Fisher's equation with non-homogeneous Dirichlet boundary conditions (Wazwaz & Gorguis, 2004; Kamrujjaman, Ahmed & Alam, 2019; Ahmed & Kamrujjaman, 2019). This equation arises in many applications of heat and mass transfer, biology, and ecology. Let us now consider the Fisher's equation

$$\begin{cases} \dfrac{\partial A(x,t)}{\partial t} = \dfrac{\partial^2 A(x,t)}{\partial x^2} + 6A(x,t)\left(1 - A(x,t)\right), & x \in \Lambda \equiv [0,1], \quad t > 0, \\ A(0,t) = \left(1 + e^{-5t}\right)^{-2}, & t > 0, \quad x \in \partial\Lambda, \\ A(1,t) = \left(1 + e^{1-5t}\right)^{-2}, & t > 0, \quad x \in \partial\Lambda, \\ A(x,0) = (1 + e^{x})^{-2}, & x \in \Lambda. \end{cases} \tag{27}$$

The exact solution of equation (27) is given by

$$A(x,t) = \left(1 + e^{x-5t}\right)^{-2}.$$

We compute the numerical solution of this problem at different nodes of x and at different time levels by using only 40 linear elements with $\alpha = 1$, $k = 0.01$, and $h = 0.025$. We reported the parallelism between exact and approximate solutions in Table 1. The graphical representation of exact and approximate solutions for different time levels are displayed in Figure 5 and in Figure 6.

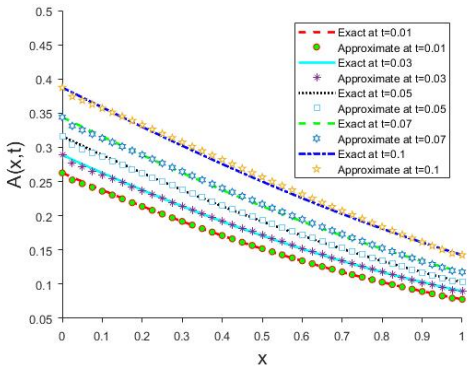

Figure 5. Comparative graphical scenarios of exact and approximate solutions of (27) at different time levels

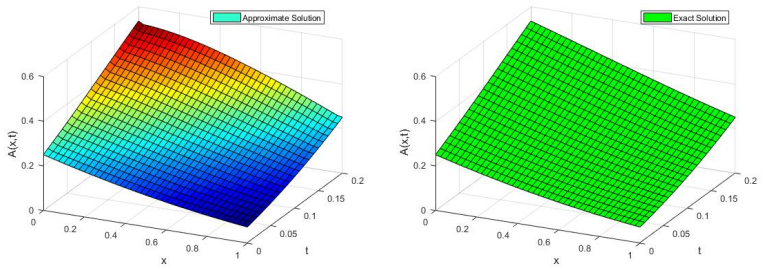

Figure 6. Approximate and exact solution of (27) over the domain while time varies

From Figure 6, we can observe that the graphical representation between the exact and approximate solution of (27). Since the approximate solution is very close to the exact solution, so from these diagrams, it is not straightforward and easy to identify the difference between them. Both solutions are exhibited by two transparent graphs concerning time and space to overcome this difficult situation.

To clarify this, let us consider the absolute error map of (27) over space using various time levels. Eventually, it is apparent that this method is more applicable for solving such types of nonlinear parabolic PDEs with a perfect consent between the approximate and exact solution of (27); Figure 6.

Table 1. Comparison of exact and approximate solutions of (27)

	$t = 0.05$			$t = 0.10$		
x	Exact	Approximate	Abs.Error	Exact	Approximate	Abs.Error
0.00	0.31604	0.31604	3.4548×10^{-17}	0.38746	0.38746	2.3036×10^{-17}
0.10	0.28581	0.28883	3.0202×10^{-03}	0.35710	0.35843	1.3277×10^{-03}
0.20	0.26186	0.26265	7.9096×10^{-04}	0.33277	0.32998	2.7832×10^{-03}
0.30	0.23826	0.23766	6.0294×10^{-04}	0.30748	0.30232	5.1643×10^{-03}
0.40	0.21532	0.21397	1.3530×10^{-03}	0.28187	0.27560	6.2664×10^{-03}
0.50	0.19331	0.19169	1.6189×10^{-03}	0.25640	0.2500	6.4044×10^{-03}
0.60	0.17240	0.17089	1.5136×10^{-03}	0.23143	0.22564	5.7870×10^{-03}
0.70	0.15270	0.15160	1.0980×10^{-03}	0.20719	0.20265	4.5391×10^{-03}
0.80	0.13424	0.13386	3.8682×10^{-04}	0.18381	0.18110	2.7125×10^{-03}
0.90	0.11701	0.11764	6.3637×10^{-04}	0.16135	0.16105	2.9391×10^{-04}
1.00	0.10293	0.10293	9.6702×10^{-18}	0.14254	0.14254	6.3233×10^{-18}

Now, we are devoted to demonstrating the famous Burgers-Huxley equation with homogeneous Neumann boundary conditions.

4.3 Burgers-Huxley Equation

Another renown nonlinear parabolic partial differential equation is the Burgers-Huxley equation with no-flux boundary conditions (Mittal & Jain, 2012; Zhou & Cheng, 2011)

$$\begin{cases} \dfrac{\partial A}{\partial t} = \dfrac{\partial^2 A}{\partial x^2} - \varphi A \dfrac{\partial A}{\partial x} + \epsilon A(x,t)\left(A(x,t)-1\right)\left(\tau - A(x,t)\right), & x \in [-25, 17], \quad t > 0, \\ \dfrac{\partial A}{\partial x}|_{x=-25} = \dfrac{\partial A}{\partial x}|_{x=17} = 0, & t > 0, \quad x \in \partial\Lambda, \\ A(x,0) = \frac{3}{2} + \frac{1}{2}\tanh\left(\dfrac{x}{2}\right), & x \in \Lambda. \end{cases} \tag{28}$$

Here φ, ϵ, and τ are real parameters. It is easily verified that the exact solution of Burgers-Huxley equations (28) is

$$A(x,t) = \frac{3}{2} + \frac{1}{2}\left[\tanh\frac{1}{2}(x+3t)\right],$$

where $\varphi = -1$, $\epsilon = 1$, and $\tau = 2$ is being used to get the numerical solution while time varies. We compute the numerical solution of the above system (28) at different nodes of x and at different time levels by using 40 linear elements with $\alpha = 1$, $k = 0.01$, and $h = 1.05$.

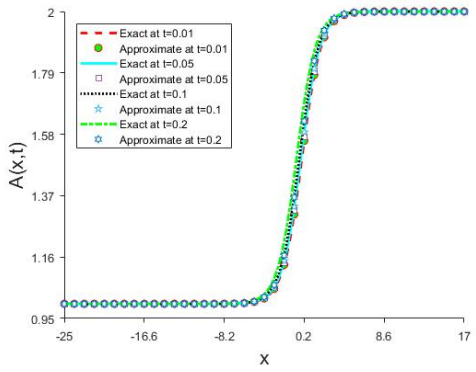

Figure 7. The profile of the solutions of (28) at different time levels over the domain

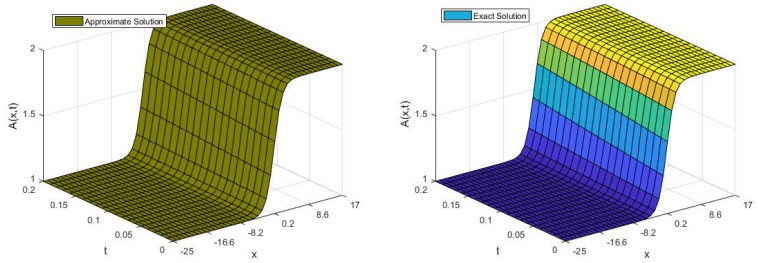

Figure 8. Approximate and Exact solution of (28) over the domain while time varies

Comparison between the exact and approximate solutions are shown in Table 2. Graphical visualizations are shown in Figure 7. The three-dimensional solutions of (28) are presented in Figure 8 where there is a good correlation between the exact and imminent solutions, which ensured the acceptance of the numerical illustrations obtained by GFEM.

Numerical simulations depicted in Figure 7 indicate that the visible exact and approximate solutions have an excellent agreement. The error curves are presented in Figure 8 and are showing the higher accuracy, which ensures the stability of this algorithm.

Table 2. Comparison of exact and approximate solutions of Burgers-Huxley equation (28)

	$t = 0.10$			$t = 0.20$		
x	Exact	Approximate	Abs.Error	Exact	Approximate	Abs.Error
-25.00	1.0000	1.0000	4.7294×10^{-13}	1.0000	1.0000	3.8443×10^{-12}
-20.80	1.0000	1.0000	1.8569×10^{-10}	1.0000	1.0000	4.0890×10^{-11}
-16.60	1.0000	1.0000	1.2383×10^{-08}	1.0000	1.0000	2.7267×10^{-09}
-12.40	1.0000	1.0000	8.2579×10^{-07}	1.0000	1.0000	1.8184×10^{-07}
-8.20	1.0003	1.0004	5.5026×10^{-05}	1.0004	1.0004	1.2109×10^{-05}
-4.00	1.0206	1.0241	3.4881×10^{-03}	1.0234	1.0241	7.1801×10^{-04}
0.20	1.5875	1.6225	3.4979×10^{-03}	1.6251	1.6225	2.6666×10^{-03}
4.40	1.9898	1.9910	1.2231×10^{-03}	1.9917	1.9910	7.5409×10^{-04}
8.60	1.9998	1.9999	1.8603×10^{-05}	1.9999	1.9999	1.1858×10^{-05}
12.80	2.0000	2.0000	2.7902×10^{-07}	2.0000	2.0000	1.7796×10^{-07}
17.00	2.0000	2.0000	8.4850×10^{-09}	2.0000	2.0000	4.1123×10^{-09}

Finally, we illustrate the Newell-Whitehead-Segel equation with non-homogeneous Neumann boundary conditions.

4.4 Newell-Whitehead-Segel Equation

Let us consider the Newell-Whitehead-Segel equation that models the interaction of the impact of the diffusion term with

the nonlinear effect of the reaction term (Salman Nourazar, Soori & Nazari-Golshan, 2015).

$$\begin{cases} \dfrac{\partial A(x,t)}{\partial t} = \eta \dfrac{\partial^2 A(x,t)}{\partial x^2} + \mu A(x,t) - \nu A(x,t)^{\rho}, & x \in \Lambda \equiv [0,1], \quad t > 0, \\ \dfrac{\partial A}{\partial x}|_{x=0} = -\dfrac{2}{\sqrt{6}} \dfrac{e^{\frac{-5t}{6}}}{\left(1+e^{\frac{-5t}{6}}\right)^3}, & t > 0, \quad x \in \partial\Lambda, \\ \dfrac{\partial A}{\partial x}|_{x=1} = -\dfrac{2}{\sqrt{6}} \dfrac{e^{\frac{\sqrt{6}-5t}{6}}}{\left(1+e^{\frac{\sqrt{6}-5t}{6}}\right)^3}, & t > 0, \quad x \in \partial\Lambda, \\ A(x,0) = \left(1+e^{\frac{x}{\sqrt{6}}}\right)^{-2}, & x \in \Lambda, \end{cases} \tag{29}$$

where η, μ, ν are real numbers with $\eta > 0$ and ρ is a positive integer. To get the approximate solution of Newell-Whitehead-Segel equation, we choose $\eta = 1$, $\mu = 1$, $\nu = 1$ and $\rho = 2$.

The exact solution of (29) is defined as

$$A(x,t) = \left(1 + e^{\frac{x}{\sqrt{6}} - \frac{5t}{6}}\right)^{-2}.$$

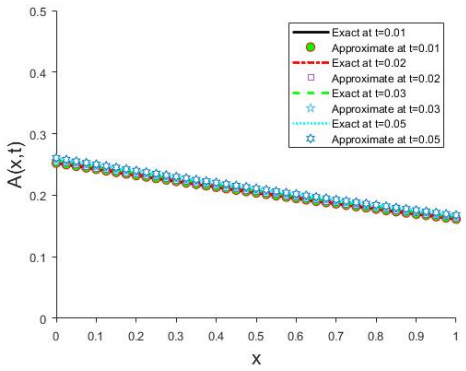

Figure 9. Comparative solutions of (29) at different time levels over the domain $x \in [0, 1]$

The numerical computations are performed using only 41 nodes with $\alpha = 1$, $k = 0.01$ and $h = 0.025$. The numerical results are presented in Table 4 (Appendix A). Additionally, the graphical visualization between the exact and approximate results is depicted in Figure 9. Visibly it is seen that the approximate and exact solutions coincide.

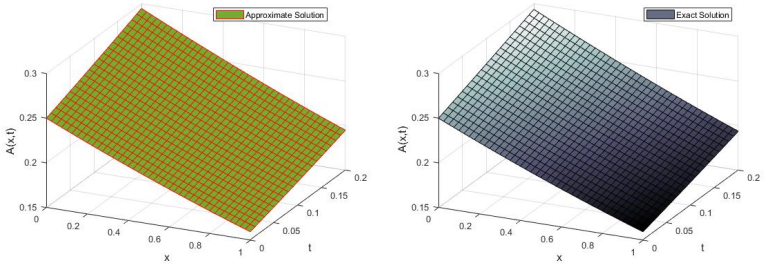

Figure 10. Approximate and exact solution of (29) over the domain while time varies

For better understanding, we also affix the 3D solution maps (Figure 10) of (29) over the independent time and space variables, which depicts the acceptability of this method by displaying high accuracy with the exact solution.

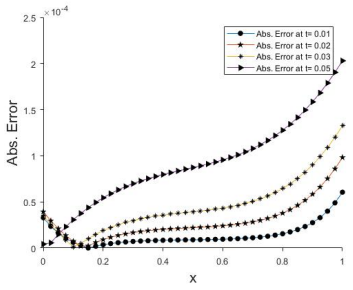

Figure 11. Absolute error of (29) at different time levels over the domain $x \in [0, 1]$

The error curves, the absolute difference between the exact and numerical solutions of (29) are presented in Figure 11. The absolute error map provided a minimal error which is acceptable for numerically illustrated results.

4.5 Problem With Robin Boundary Condition

Let us consider the uniformly propagating shock problem (Sapa, 2018)

$$\begin{cases} \dfrac{\partial A(x,t)}{\partial t} = \frac{1}{Re}\dfrac{\partial^2 A(x,t)}{\partial x^2} - A(x,t)\dfrac{\partial A(x,t)}{\partial x}, & x \in \Lambda \equiv [-1,1], \quad t > 0, \\ A(-1,t) + \dfrac{\partial A(-1,t)}{\partial x} = \dfrac{t^2+8t+13}{(t+3)^2}, & t > 0, \quad x \in \partial\Lambda, \\ A(1,t) - \dfrac{\partial A(1,t)}{\partial x} = \dfrac{t^2+4t+5}{(t+1)^2}, & t > 0, \quad x \in \partial\Lambda, \\ A(x,0) = \frac{x-4}{x-2}, & x \in \Lambda. \end{cases} \tag{30}$$

The exact solution of this problem (30) is $A(x,t) = 1 - \frac{2}{x-t-2}$.

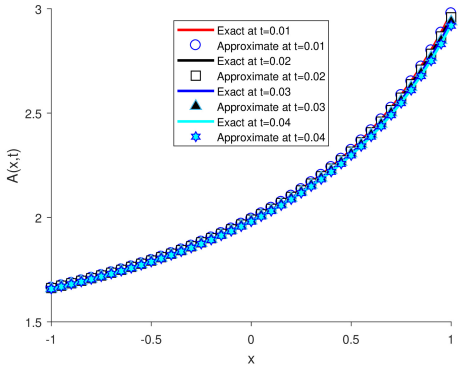

Figure 12. Comparative solutions of (30) at different time levels over the domain $x \in [-1, 1]$

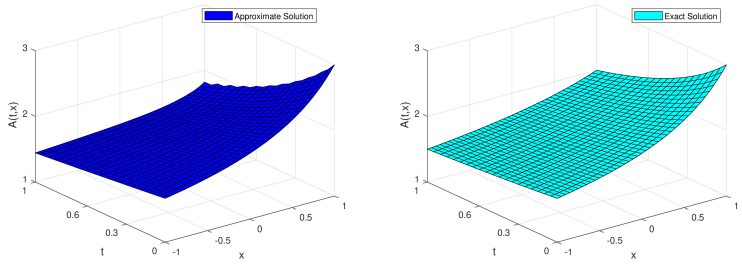

Figure 13. Approximate and exact solution of (30) over the domain while time varies

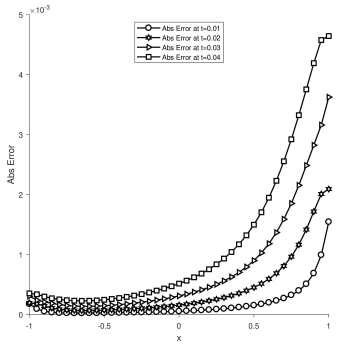

Figure 14. Absolute error of (30) at different time levels over the domain $x \in [-1, 1]$

Here Re is the Reynolds number in the range $1 \leq Re \leq 10^5$ and for $(x, t) \in [-1, 1] \times [0, 1]$, $A(x, t) \in (1.5, 3)$. Graphical representations are given in Figures 12, 13, 14.

5. Conclusion

In this study, an efficient scheme based on the Galerkin finite element method has been introduced to find the numerical solutions of a general class of nonlinear parabolic partial differential equations with different boundary conditions. The method was applied directly to find the approximate solutions of the equations without any limitations; it excluded linearization technique, no further assumption on trial functions, and no need to transform into lower-order PDE. To verify the method, we recalled several real-life problems, such as Burger's equation, Newell-Whitehead-Segel equation, and additional two renowned PDEs where all the equations carried out various boundary conditions. The approximate results were compared with the exact solutions and presented graphically (2D & 3D) and in tabular form. By the way of conclusion, it is apparent about the efficiency, accuracy, and acceptance of the proposed scheme because of its low cost, easily implementable, high accuracy with low compuatation time compared to the well-published literature.

Acknowledgment

The authors are grateful to the anonymous reviewers for their constructive suggestions and comments to improve the quality of the paper significantly. The authors M. S. Islam and H. Ali are grateful to the centennial research program, Dhaka University. All authors acknowledged to the University of Dhaka for their research support.

Conflict of Interest

The authors declare that they have no conflict of interest.

Author contributions

Conceptualization, H.A. and M.K.; methodology, H.A., M.K and M.S.I; software, H.A; validation, H.A.; formal analysis, H.A. and M.K; investigation, M.S.I.; resources, M.S.I. and M.K.; data curation, H.A. and M.K.; original draft preparation, H.A.; review and editing, M.K. and M.S.I.; supervision, M.K. All authors have read and agreed to the published version of the manuscript.

References

Ahmed, A., & Kamrujjaman, M. (2019). Analytic Travelling Wave Solutions and Numerical Analysis of Fisher's Equation via Explicit-Implicit FDM. Asian Journal of Advanced Research and Reports, 1-13.

Akter, S. I., Mahmud, M. S., Kamrujjaman, M., & Ali, H. (2020). Global Spectral Collocation Method with Fourier Transform to Solve Differential Equations. *GANIT: Journal of Bangladesh Mathematical Society, 40*(1), 28-42. https://doi.org/10.3329/ganit.v40i1.48193

Ali, H., & Islam, M. S. (2017). Generalized Galerkin finite element formulation for the numerical solutions of second order nonlinear boundary value problems. *GANIT: Journal of Bangladesh Mathematical Society, 37*, 147-159. https://doi.org/10.3329/ganit.v37i0.35733

Ali, H., Kamrujjaman, M., & Islam, M. S. (2020). Numerical Computation of Fitzhugh-Nagumo Equation: A Novel Galerkin Finite Element Approach. *International Journal of mathematical research, 9*(1), 20-27.

Ali, H., Kamrujjaman, M., & Shirin, A. (2021). Numerical solution of a fractional-order Bagley-Torvik equation by quadratic finite element method. *Journal of Applied Mathematics and Computing, 66*(1), 351-367.

https://doi.org/10.1007/s12190-020-01440-6

Ali, H., & Kamrujjaman, M. (2021), Numerical solutions of nonlinear parabolic equations with Robin condition: Galerkin approach, *Journal of Applied and Engineering Mathematics*, in press.

Babuska, I. (1972). Survey lectures on the mathematical foundations of the finite element method. The Mathematical Foundations of the Finite Element Method with Applicaions to Partial Differential Equations, 3-359.

Babuska, I., & Rheinboldt, W. C. (1978). A posteriori error estimates for the finite element method. *International Journal for Numerical Methods in Engineering, 12*(10), 1597-1615. https://doi.org/10.1002/nme.1620121010

Caldwell, J., Wanless, P., & Cook, A. E. (1981). A finite element approach to Burgers' equation. *Applied Mathematical Modelling, 5*(3), 189-193. https://doi.org/10.1016/0307-904X(81)90043-3

Chen, Z. (2005). Semiconductor Modeling. *Finite Element Methods and Their Applications*, 363-384. https://doi.org/10.1007/3-540-28078-2_10

Cherniha, R., & Dutka, V. (2001). Exact and numerical solutions of the generalized Fisher equation. *Reports on Mathematical Physics, 47*(3), 393-411. https://doi.org/10.1016/S0034-4877(01)80052-5

Jacques, I. B. (1983). Predictor-corrector methods for parabolic partial differential equations. *International Journal for Numerical Methods in Engineering, 19*(3), 451-465. https://doi.org/10.1002/nme.1620190311

Kamrujjaman, M., Ahmed, A., & Alam, J. (2019). Travelling Waves: Interplay of Low to High Reynolds Number and Tan-Cot Function Method to Solve Burgers Equations. *Journal of Applied Mathematics and Physics, 7*(04), 861.

Lewis, P. E., & Ward, J. P. (1991). *The finite element method: principles and applications* (pp. 26-41). Wokingham: Addison-Wesley.

Lima, S. A., Kamrujjaman, M., & Islam, M. S. (2020). Direct Approach to Compute a Class of Reaction-Diffusion Equation by a Finite Element Method. *Journal of Applied Mathematics and Computation, 4*(2), 26-33.

Lima, S. A., Kamrujjaman, M., & Islam, M. S. (2021). Numerical solution of convection-diffusion-reaction equations by a finite element method with error correlation. *AIP Advances, 11*(8), 085225.

Mittal, R. C., & Jain, R. K. (2012). Cubic B-splines collocation method for solving nonlinear parabolic partial differential equations with Neumann boundary conditions. *Communications in Nonlinear Science and Numerical Simulation, 17*(12), 4616-4625. https://doi.org/10.1016/j.cnsns.2012.05.007

Ozis, T., Aksan, E. N., & Ozdes, A. (2003). A finite element approach for solution of Burgers equation. *Applied Mathematics and Computation, 139*(2-3), 417-428. https://doi.org/10.1016/S0096-3003(02)00204-7

Rao, S. S. (2017). The finite element method in engineering. Butterworth-heinemann.

Reddy, J. N. (2014). An Introduction to Nonlinear Finite Element Analysis Second Edition: with applications to heat transfer, fluid mechanics, and solid mechanics. OUP Oxford.

Salman Nourazar, S., Soori, M., & Nazari-Golshan, A. (2015). On The Exact Solution of Newell-Whitehead-Segel Equation Using the Homotopy Perturbation Method. arXiv e-prints, arXiv-1502.

Sapa, L. (2018). Difference methods for parabolic equations with Robin condition. *Applied Mathematics and Computation, 321*, 794-811. https://doi.org/10.1016/j.amc.2017.10.061

Wazwaz, A. M., & Gorguis, A. (2004). An analytic study of Fisher's equation by using Adomian decomposition method. *Applied Mathematics and Computation, 154*(3), 609-620. https://doi.org/10.1016/S0096-3003(03)00738-0

Wood, W. L. (2006). An exact solution for Burger's equation. *Communications in numerical methods in engineering, 22*(7), 797-798. https://doi.org/10.1002/cnm.850

Zhou, S., & Cheng, X. (2011). A linearly semi-implicit compact scheme for the Burgers Huxley equation. *International Journal of Computer Mathematics, 88*(4), 795-804. https://doi.org/10.1080/00207161003743391

Hassan, H., & Rashidi, M. M. (2014). An analytic solution of micropolar flow in a porous channel with mass injection using homotopy analysis method. *International Journal of Numerical Methods for Heat & Fluid Flow, 24*(2), 419-437. https://doi.org/10.1108/HFF-08-2011-0158

Sarwar, S., & Rashidi, M. M. (2016). Approximate solution of two-term fractional-order diffusion, wave-diffusion, and telegraph models arising in mathematical physics using optimal homotopy asymptotic method. *Waves in random and complex media, 26*(3), 365-382. https://doi.org/10.1080/17455030.2016.1158436

A. Appendix

This section contains some additional figures and tables to observe the accuracy of the solution methodology; the Galerkin Finite Element Method.

Table 3. Comparison of exact and approximate solutions of equation (26)

	$t = 0.02$			$t = 0.04$		
x	Exact	Approximate	Abs.Error	Exact	Approximate	Abs.Error
0.00	0.00	0.00	0.00	0.00	0.00	0.00
0.10	0.5690	0.5732	4.2015×10^{-03}	0.4833	0.4954	1.2084×10^{-02}
0.20	1.1289	1.1379	9.0897×10^{-03}	0.9528	0.9778	2.4978×10^{-02}
0.30	1.6658	1.6808	1.5057×10^{-02}	1.3909	1.4295	3.8572×10^{-02}
0.40	2.1549	2.1766	2.1634×10^{-02}	1.7727	1.8234	5.0734×10^{-02}
0.50	2.5523	2.5788	2.6538×10^{-02}	2.0605	2.1169	5.6374×10^{-02}
0.60	2.7838	2.8089	2.5080×10^{-02}	2.1990	2.2472	4.8259×10^{-02}
0.70	2.7370	2.7497	1.2625×10^{-02}	2.1127	2.1355	2.2751×10^{-02}
0.80	2.2762	2.2693	6.8314×10^{-03}	1.7197	1.7105	9.1888×10^{-03}
0.90	1.3219	1.3071	1.4806×10^{-02}	0.9832	0.9626	2.0606×10^{-02}
1.00	0.00	0.00	0.00	0.00	0.00	0.00

Table 4. Comparison of exact and approximate solutions of Newell-Whitehead-Segel equation (29)

	$t = 0.03$			$t = 0.05$		
x	Exact	Approximate	Abs.Error	Exact	Approximate	Abs.Error
0.00	0.256288733	0.256253420	3.531×10^{-05}	0.260523635	0.260519434	4.201×10^{-06}
0.10	0.246059526	0.246058049	1.477×10^{-06}	0.250210503	0.250241120	3.062×10^{-05}
0.20	0.236041838	0.236060682	1.884×10^{-05}	0.240105472	0.240159946	5.447×10^{-05}
0.30	0.226243545	0.226273433	2.989×10^{-05}	0.230216706	0.230286547	6.984×10^{-05}
0.40	0.216671793	0.216707468	3.568×10^{-05}	0.220551653	0.220631376	7.972×10^{-05}
0.50	0.207332982	0.207372295	3.931×10^{-05}	0.211117020	0.211204262	8.724×10^{-05}
0.60	0.198232752	0.198276112	4.336×10^{-05}	0.201918757	0.202014293	9.554×10^{-05}
0.70	0.189375975	0.189426519	5.054×10^{-05}	0.192962052	0.193069916	1.079×10^{-04}
0.80	0.180766749	0.180831245	6.450×10^{-05}	0.184251318	0.184379006	1.277×10^{-04}
0.90	0.172408404	0.172498494	9.009×10^{-05}	0.175790198	0.175948651	1.585×10^{-04}
1.00	0.164303506	0.164436046	1.325×10^{-04}	0.167581569	0.167784547	2.030×10^{-04}

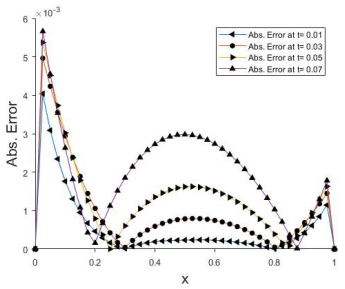

Figure 15. Error graph of (27) at different time levels over the domain

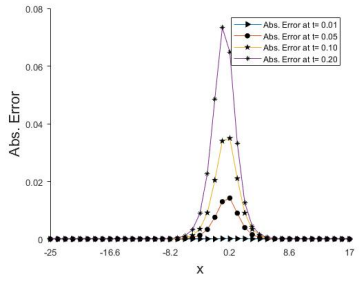

Figure 16. The absolute error of (28) at different time levels over the domain